



Magnetic polymer-supported adsorbent with two functional adsorption sites for phosphate removal

Ting Li¹ · Pengwei Huang¹ · Taiwan Liao¹ · Jia Guo² · Xiang Yu³ · Boping Han⁴ · Liang Peng⁴ · Yi Zhu¹ · Yuanming Zhang¹

Received: 27 May 2019 / Accepted: 29 August 2019 / Published online: 13 September 2019
© Springer-Verlag GmbH Germany, part of Springer Nature 2019

Abstract

In this paper, a new magnetic polymer-supported phosphate adsorbent MPVC-EDA-Ce was prepared by loading cerium (hydr)oxides onto ethylenediamine-functionalized polyvinyl chloride for the first time. MPVC-EDA-Ce showed excellent adsorption performances towards phosphate and easy recovery. The adsorption isotherm and kinetics of MPVC-EDA-Ce followed Langmuir monolayer model and the pseudo-second-order model, respectively. The pH results demonstrated that the MPVC-EDA-Ce could effectively remove phosphate in a wide range of pH with insignificant cerium leaching. Furthermore, analyses on adsorption mechanism and effect of competing anions demonstrated the formation of strong inner-sphere complexation between cerium (hydr)oxides and phosphate, which was a selective adsorption process, while positively charged quaternary ammonium groups adsorbed phosphate via relatively weak electrostatic attraction which was a non-selective adsorption process. The study provided a good reference to design novel phosphate adsorbents with two even more functional adsorption sites and a deep insight to investigate the adsorption mechanism towards phosphate.

Keywords Functionalized polyvinyl chloride · Cerium (hydr)oxides · Quaternary ammonium groups · Two functional adsorption sites · Phosphate removal

Introduction

Removal of excessive phosphate from waterbodies has become an urgent problem receiving widespread attention, which will deteriorate water quality, cause eutrophication,

and disrupt the aquatic ecological environment (Robalds et al. 2016; Shen et al. 2019). Numerous methods (e.g., chemical precipitation, adsorption, reverse osmosis, and biological removal) have been reported to remove phosphate, among which adsorption is regarded as one of the most promising methods to remove phosphate due to its low cost, high removal efficiency, easy operation, and no production of secondary contaminants. Various waste materials, natural and synthetic materials, have been used as phosphate adsorbents in wastewater treatment. For example, industrial waste materials such as fly ash (Goscianska et al. 2018), natural materials such as natural clay (Tian et al. 2009; Gan et al. 2009), synthetic materials such as metal cations/(hydr)oxides, iron-based adsorbents (Zhou et al. 2016), and iron oxide tailing (Zeng et al. 2004) have been reported.

Metal compounds such as metal cations/(hydr)oxides and complexes have been utilized as adsorbents for phosphate removal for decades. Especially, compounds of cerium have been considered as desirable adsorbents for phosphate due to their abundance, cheapness, and excellent adsorption performance towards phosphate resulting from high affinities towards anions (Su et al. 2015). For example, Su et al. (2015)

Responsible editor: Tito Roberto Cadaval Jr

Electronic supplementary material The online version of this article (<https://doi.org/10.1007/s11356-019-06351-z>) contains supplementary material, which is available to authorized users.

✉ Yi Zhu
tzhury@jnu.edu.cn

¹ Department of Chemistry, Jinan University, Guangzhou 510632, People's Republic of China

² Department of Ecology, Jinan University, Guangzhou 510632, People's Republic of China

³ Analytical & Testing Center, Jinan University, Guangzhou 510632, People's Republic of China

⁴ Institute of Hydrobiology, Jinan University, Guangzhou 510632, People's Republic of China

synthesized cerium-zirconium binary oxide nanoparticles for phosphate removal and found that the adsorption amount of phosphate was larger when the content of cerium in the adsorbent was higher than that of zirconium. Hong et al. (2017) fabricated a hybrid adsorbent $\text{Fe}_3\text{O}_4@\text{SiO}_2@m\text{CeO}_2$ and found that mesoporous CeO_2 with large specific surface area could provide many adsorption sites, which facilitated improving the adsorption capacity for phosphate. It would be a good method to load cerium onto host materials to avoid excessive consumption of cerium (Feng et al. 2017). For example, Hu et al. (2017) prepared a Ce(III)-impregnated cross-linked chitosan complex as a phosphate adsorbent, which possessed excellent adsorption performance towards phosphate.

The quaternary ammonium groups were confirmed to be the excellent adsorption sites for phosphate and usually loaded onto host materials. For example, Qiu et al. (2015) fabricated biomass-based Ws-N-Zr by immobilizing hydrous zirconium oxide nanoparticle in quaternary-aminated wheat straw, in which the quaternary ammonium groups immobilized onto the host materials favored the phosphate adsorption onto the wheat straw. Bui et al. (2018) prepared a hybrid adsorbent of zirconium molybdate bonded on a macroporous anion exchange resin and found that the quaternary ammonium groups of the anion exchange resin provided adsorption sites for phosphate.

As a kind of synthetic polymer material with low cost, good stability, and high reversibility, polyvinyl chloride was often used as the host material to be functionalized with catalytically active sites by direct loading in the preparation of catalysts (Samarasimhareddy et al. 2013; Yoo and Kwak 2011). Correspondingly, polyvinyl chloride can also be used as the host material to be functionalized by loading adsorption sites towards phosphate, which could be modified by quaternary ammonium groups, using ethylenediamine (EDA). So far, there was no information about the use of modified polyvinyl chloride as phosphate adsorbent.

For powder adsorbents, a distinct disadvantage is the difficulty to be separated from solution. Magnetic separation, with various advantages of easy operation, high efficiency, and low cost, is a good solution for this problem. Iron oxide was used as magnetic medium and added to the powder adsorbents to form magnetic composites, which could easily be separated from the solution by magnetic field (Long et al. 2011; Yoon et al. 2014).

In this research, both functional adsorption sites (quaternary ammonium groups and cerium (hydr)oxides) were loaded to polyvinyl chloride (PVC), which was a kind of synthetic polymer material used as the host material due to low cost, good stability, and high reversibility, to construct a novel adsorbent with two functional adsorption sites towards phosphate. The chlorine atom on the molecular chain of polyvinyl chloride was substituted by ethylenediamine (EDA) to obtain functionalized polyvinyl chloride (PVC-EDA). Iron oxide was then deposited onto rather than bonded with PVC-EDA to form magnetic PVC-EDA (MPVC-EDA), which facilitated

the recovery of the adsorbents from the aqueous solution (Hong et al. 2017; Markeb et al. 2016). Finally, the amine of MPVC-EDA chelated with metal ion cerium, which was then heated to cerium (hydr)oxides, and MPVC-EDA-Ce was obtained. Adsorption kinetics and isotherm were investigated. The influences of the solution pH and competing anions on phosphate adsorption were examined. Moreover, the contributions of each functional site (quaternary ammonium groups and cerium (hydr)oxides) to the adsorption towards phosphate were studied and quantified. The underlying adsorption mechanism was further revealed.

Materials and methods

Reagents and materials

The chemicals were all analytical grade of reagent. Cerium chloride heptahydrate, polyvinyl chloride, and potassium dihydrogen phosphate were provided by Aladdin Biochemical Technology Co., Ltd. (Shanghai, China). Ethylenediamine, ferric chloride hexahydrate, sodium hydrate, sodium chloride, ferrous chloride tetrahydrate, trisodium citrate, sodium sulfate, hydrochloric acid, and sodium nitrate were provided by Guangzhou Chemical Reagent Station. Cerium phosphate hydrate was provided by Saan Chemical Technology Co., Ltd. (Shanghai, China).

Preparation of materials

In order to prepare the functionalized polyvinyl chloride, 20 g of polyvinyl chloride (PVC) and 80 mL of ethylenediamine (EDA) were added to a round-bottomed flask. After placing at room temperature for 24 h, some distilled water (5 mL) was added into the mixture followed by heating for 48 h under electromagnetic stirring at 80 °C; then, the sample was washed by using plenty of distilled water to remove ethylenediamine. Finally, it was dried at 80 °C to obtain an ethylenediamine-functionalized polyvinyl chloride (PVC-EDA) in the form of reddish brown powder.

For the synthesis of magnetically ethylenediamine-functionalized polyvinyl chloride (MPVC-EDA), 4 g PVC-EDA powder, 2.4 g $\text{FeCl}_2\cdot 4\text{H}_2\text{O}$, and 3.2 g $\text{FeCl}_3\cdot 6\text{H}_2\text{O}$ were dissolved in distilled water (60 mL), which was then magnetically stirred for 0.5 h at 60 °C. Then, the solution pH was adjusted to 11 using 1 mol/L NaOH. After adding 0.25 g of trisodium citrate, the above solution was heated to 80 °C and constantly stirred for 1 h followed by being filtered, rinsed, and dried and finally MPVC-EDA was obtained.

For the synthesis of magnetically ethylenediamine-functionalized polyvinyl chloride-loaded cerium (MPVC-EDA-Ce), 2 g of MPVC-EDA was dissolved in 20 mL of ethanol solution (95%) followed by being placed at room

temperature for 2 h. After the addition of CeCl₃·7H₂O (2.98 g), the mixture was heated for 48 h under electromagnetic stirring at 80 °C followed by being filtered and rinsed using distilled water. Finally, the cerium was successfully loaded onto the magnetically ethylenediamine-functionalized polyvinyl chloride after being dried at 80 °C overnight.

Adsorbent characterization

The Brunauer-Emmett-Teller (BET) method was used to calculate the specific surface areas via N₂ adsorption studies on a ASAP 2010 (Micromeritics Inc., USA). The Fourier transform infrared (FT-IR) spectrometer (Nicolet iS50 FT-IR, USA) was used to analyze surface functional groups of the samples by ATR mode. The morphologies and elemental compositions of the sample surfaces were analyzed after adsorption experiments without being washed via the scanning electron microscopy (SEM, Zeiss ULTRA 55) combined with energy dispersive spectroscopy (EDS, Bruker/Quanta 200), and the X-ray photoelectron spectroscopy (XPS, ESCALab-250) was also used to study the surface elements. The vibrating sample magnetometer (VSM, LAKESHORE 7407) was used to examine the magnetic properties of the samples. The zeta potential analyzer (NANO ZS90, Malvern, UK) was used to study the point of zero charge (PZC). The concentrations of ions from the solution were measured through an inductively coupled plasma (ICP) spectrometer (iCAP 7000 SERIES), which was completed by MS.

Bath experiments

The adsorption isotherms of MPVC-EDA-Ce towards phosphate were conducted by dispersing the adsorbent (0.025 g) into different concentrations of phosphate solutions (10–80 mg P/L, 25 mL) and compared with MPVC-EDA and PVC-EDA. The mixture was shaken for 24 h at a fix temperature (30 °C). The equilibrium adsorption amount (q_e , mg/g) for phosphate was determined according to Eq. (1).

$$q_e = (V/m) \times (C_e - C_o) \tag{1}$$

where V was the solution volume (L); C_e and C_o (mg/L) represented the concentration of phosphate at equilibrium time and initial time; m was the mass of adsorbent (g).

Meanwhile, the isotherm models (i.e., Langmuir and Freundlich) were adopted to analyze the isotherm data and expressed as the following equations:

$$\frac{C_e}{q_e} = \frac{1}{k_L} \cdot \frac{1}{q_m} + \frac{C_e}{q_m} \tag{2}$$

$$q_e = k_F C_e^{1/n} \tag{3}$$

where k_L and k_F were constants associated with the affinity of binding sites and adsorption capacity, respectively; q_m represented the maximum amount (mg/g); $1/n$ expressed the adsorption intensity.

The adsorption kinetics of phosphate on MPVC-EDA-Ce were accessed by adding 1.0 g of MPVC-EDA-Ce to the aqueous solution of phosphate (50 mg P/L, 100 mL) under pH 5.0. A certain amount of the above solution was taken out and used to calculate the adsorption capacity of phosphate by ICP-MS at 0.083, 0.167, 0.333, 0.5, 1, 2, 4, 6, 8, and 12 h, respectively. To better analyze the kinetic data, the pseudo-first-order model (Eq. (4)), pseudo-second-order model (Eq. (5)), the intra-particle diffusion model (Eq. (6)), and the Boyd (Eq. (7)) model were adopted and expressed as the following equations:

$$\log(q_e - q_t) = \log q_e - \frac{k_1 t}{2.303} \tag{4}$$

$$\frac{t}{q_t} = \frac{1}{k_2 q_e^2} + \frac{t}{q_e} \tag{5}$$

$$q_t = k_d t^{1/2} + C \tag{6}$$

$$B_t = -0.4977 - \ln(1 - F) \tag{7}$$

where q_t (mg/g) was the adsorption capacity at any time; C was a constant associated with the thickness of boundary layer; k_1 (h⁻¹), k_2 (g mg⁻¹ h⁻¹), and k_d (mg g⁻¹ h^{0.5}) were the associated rate constants; F was the fraction of solute adsorbed at different times.

The influences of solution pH on phosphate adsorption were studied by dissolving MPVC-EDA-Ce (0.025 g) into the phosphate solution (50 mg P/L, 25 mL) followed by adding 0.1 mol/L HCl or NaOH solution to adjust the pH values (3–11). In addition, the concentrations of metal ions were also measured to study the stability of MPVC-EDA-Ce.

The effects of competitive ions on the amount of phosphate adsorbed were investigated by dissolving a certain amount of sodium sulfate, sodium chloride, and sodium nitrate to the phosphate solution (50 mg P/L, 50 mL). The molar amounts of the competing ions were set to be 5–10 times higher than those of the phosphate ions.

Results and discussion

XRD and FT-IR study

Figure 1 a shows the XRD patterns of PVC, PVC-EDA, MPVC-EDA, and MPVC-EDA-Ce. XRD patterns showed that

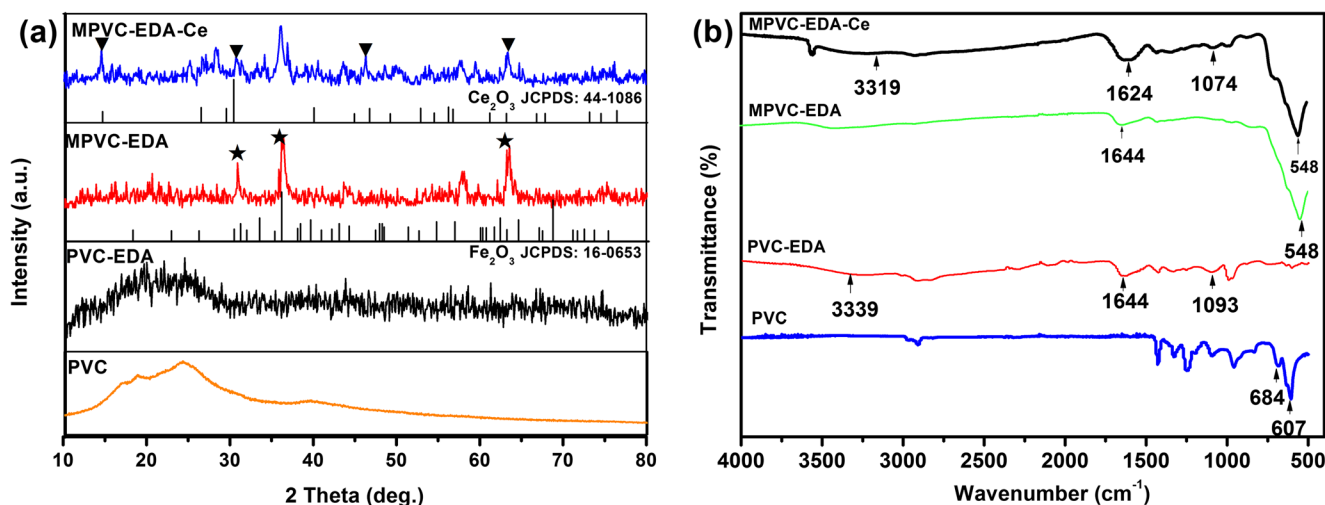


Fig. 1 XRD patterns (a) and FT-IR spectrum (b) of PVC, PVC-EDA, MPVC-EDA, and MPVC-EDA-Ce

the main peaks were mostly consistent with Ce_2O_3 (JCPDS card no. 44-1086) and Fe_2O_3 (JCPDS card no. 16-0653), indicating that iron and cerium were present in the adsorbent.

Figure 1 b depicted the FT-IR spectra of PVC, PVC-EDA, MPVC-EDA, and MPVC-EDA-Ce. The bands at 607 and 684 cm^{-1} represented the characteristic peaks of C-Cl on PVC, while there were almost no peaks of C-Cl in curve of PVC-EDA, because Cl was replaced by EDA. For PVC-EDA, the peaks of N-H (1644 and 3339 cm^{-1}) and C-N (1093 cm^{-1}) appeared, which indicated that EDA has been successfully loaded onto the PVC. For MPVC-EDA, the Fe-O lattice vibration peak around 548 cm^{-1} was observed for magnetic iron oxide. For MPVC-EDA-Ce, the peaks of N-H and C-N were located at 1624, 3319, and 1074 cm^{-1} , respectively. By comparing the curves of PVC-EDA and MPVC-EDA-Ce, the change of peak positions of N-H and C-N indicated that iron and cerium have been successfully loaded onto the MPVC-EDA-Ce.

Adsorption isotherm

Figure 2 shows the comparison of the adsorption abilities of PVC-EDA, MPVC-EDA, and MPVC-EDA-Ce towards phosphate at different equilibrium concentrations. The amount of phosphate adsorbed by PVC-EDA, MPVC-EDA, and MPVC-EDA-Ce increased with the increase of initial phosphate concentration and eventually reached equilibrium. The experimental data of PVC-EDA, MPVC-EDA, and MPVC-EDA-Ce could be fitted better by the Langmuir isotherm model ($R^2 > 0.9$) than the Freundlich isotherm model (Table 1), suggesting the monolayer adsorption for phosphate on the surface of adsorbents (Han et al. 2017; Xiong et al. 2017). The maximum adsorption amount of MPVC-EDA-Ce towards phosphate (26.18 mg/g) determined by the Langmuir model was higher as compared with that of PVC-EDA ($q_{\text{max}} = 18.20$ mg/g) and MPVC-EDA ($q_{\text{max}} = 10.32$ mg/g) (Table S1).

Comparison of adsorption capacity of other similar adsorbents for phosphate removal (Table S2) indicated the relatively good adsorption performance of MPVC-EDA-Ce. Meanwhile, it was noticed that the phosphate removal rate of MPVC-EDA-Ce could reach 99.9% even at low concentration of 10 mg P/L, indicating the potential use of MPVC-EDA-Ce in removing phosphate of low concentration (Yang et al. 2018). Hence, the following experiments were performed using MPVC-EDA-Ce as an adsorbent.

In addition, the specific surface areas of PVC-EDA, MPVC-EDA, and MPVC-EDA-Ce were 0.26, 13.39, and 15.02 m^2/g , respectively (Table S1). PVC-EDA had a lower surface area than that of MPVC-EDA, while MPVC-EDA and MPVC-EDA-Ce exhibited similar surface areas. But the order of the phosphate adsorption capacity was MPVC-EDA-Ce > PVC-EDA > MPVC-EDA. The results indicated that surface area insignificantly affected the adsorption capacity of the

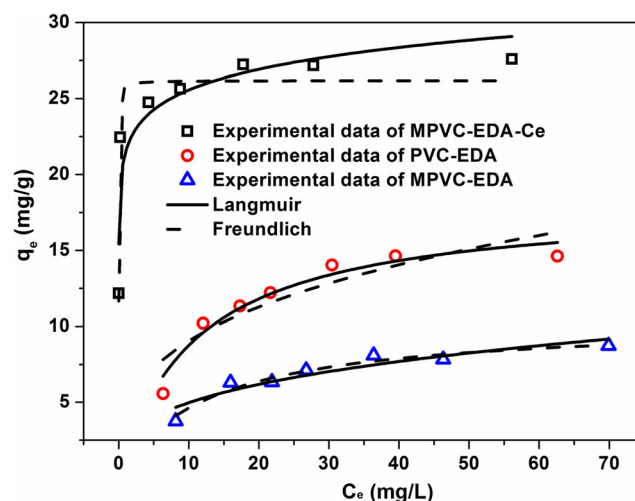


Fig. 2 Adsorption isotherms of phosphate on PVC-EDA, MPVC-EDA, and MPVC-EDA-Ce

Table 1 Langmuir and Freundlich isotherm parameters for phosphate adsorption on PVC-EDA, MPVC-EDA, and MPVC-EDA-Ce

Sample	Langmuir			Freundlich		
	q_m (mg/g)	K_L (L/mg)	R^2	n	K_F (mg/g)	R^2
PVC-EDA	18.20	0.092	0.94	3.14	4.34	0.80
MPVC-EDA	10.32	0.081	0.95	3.18	2.41	0.86
MPVC-EDA-Ce	26.18	68.29	0.93	13.36	21.51	0.83

adsorbents. The mechanism of adsorption will be further discussed in the following section.

SEM analysis

As presented in Fig. 3 a and c, the surface of MPVC-EDA-Ce before and after adsorption was apparently irregular. The EDS map results (Fig. S5) indicated Fe₂O₃ and Ce (hydr)oxides were located. The appearance of element P in MPVC-EDA-Ce after adsorption (Fig. 3c, d) suggests phosphate was effectively adsorbed onto MPVC-EDA-Ce (Du et al. 2017).

Adsorption kinetics

The amount of phosphate adsorbed by MPVC-EDA-Ce as a function of reaction time is described in Fig. 4a. The phosphate adsorption occurred rapidly and reached around 90% of the equilibrium adsorption amount after 30-min reaction time (Sendrowski and Boyer 2013). The adsorption rate gradually decreased as time increased and eventually reached equilibrium (Jung et al. 2015). Figure 4 a and Table 2 show that the adsorption kinetics of MPVC-EDA-Ce towards phosphate was interpreted by the pseudo-first-order and the pseudo-second-order models, and the correlation coefficient of the pseudo-second-order model ($R^2 = 0.978$) was greater as compared with that of the pseudo-first-order model ($R^2 = 0.921$), indicating that the pseudo-second-order model could fit better the kinetic data; hence, a chemical process may occur between the phosphate and the adsorbent (Qiu et al. 2019; Rathod et al. 2014).

Accordingly, since it was hard to describe the diffusion mechanisms using the above two kinetic models, the experimental data was also interpreted using the intra-particle diffusion model. Figure 4 b and Table 2 show the multi-linearity for

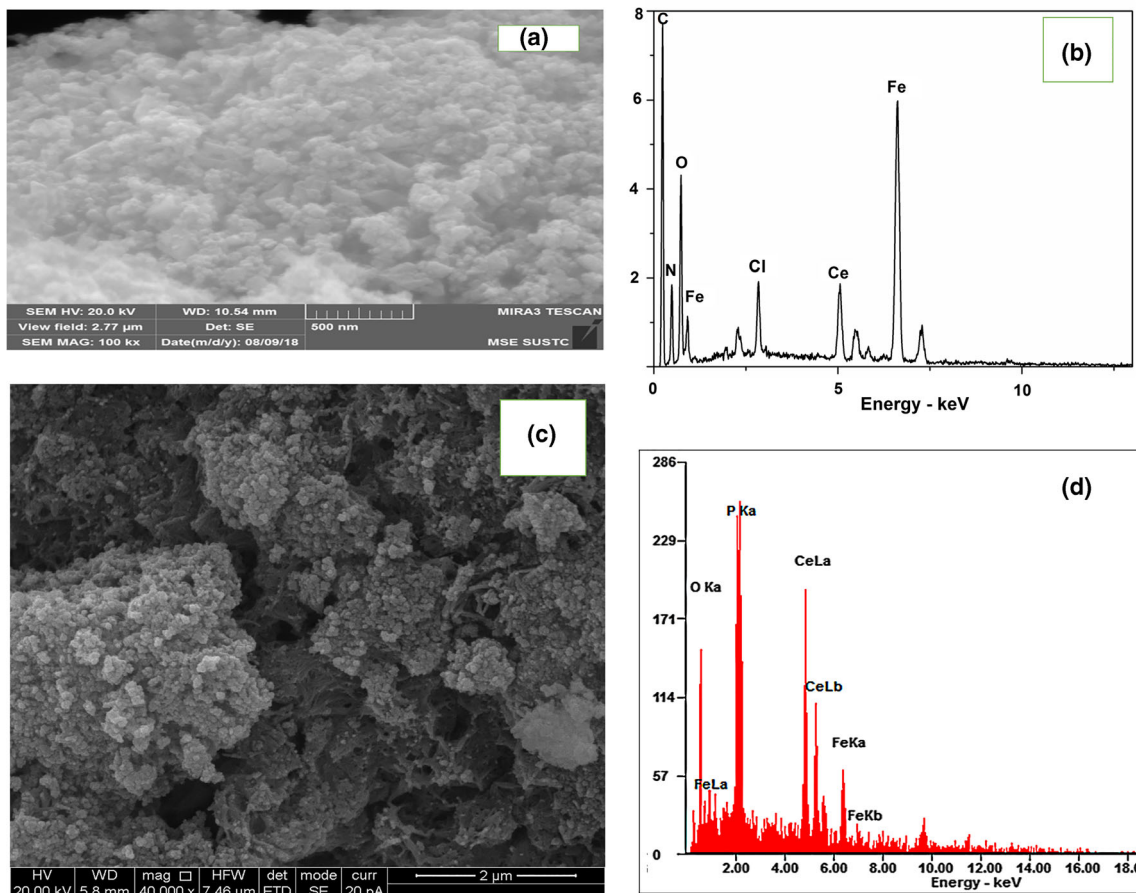


Fig. 3 SEM-EDS images of MPVC-EDA-Ce. a, b Before adsorption. c, d After adsorption

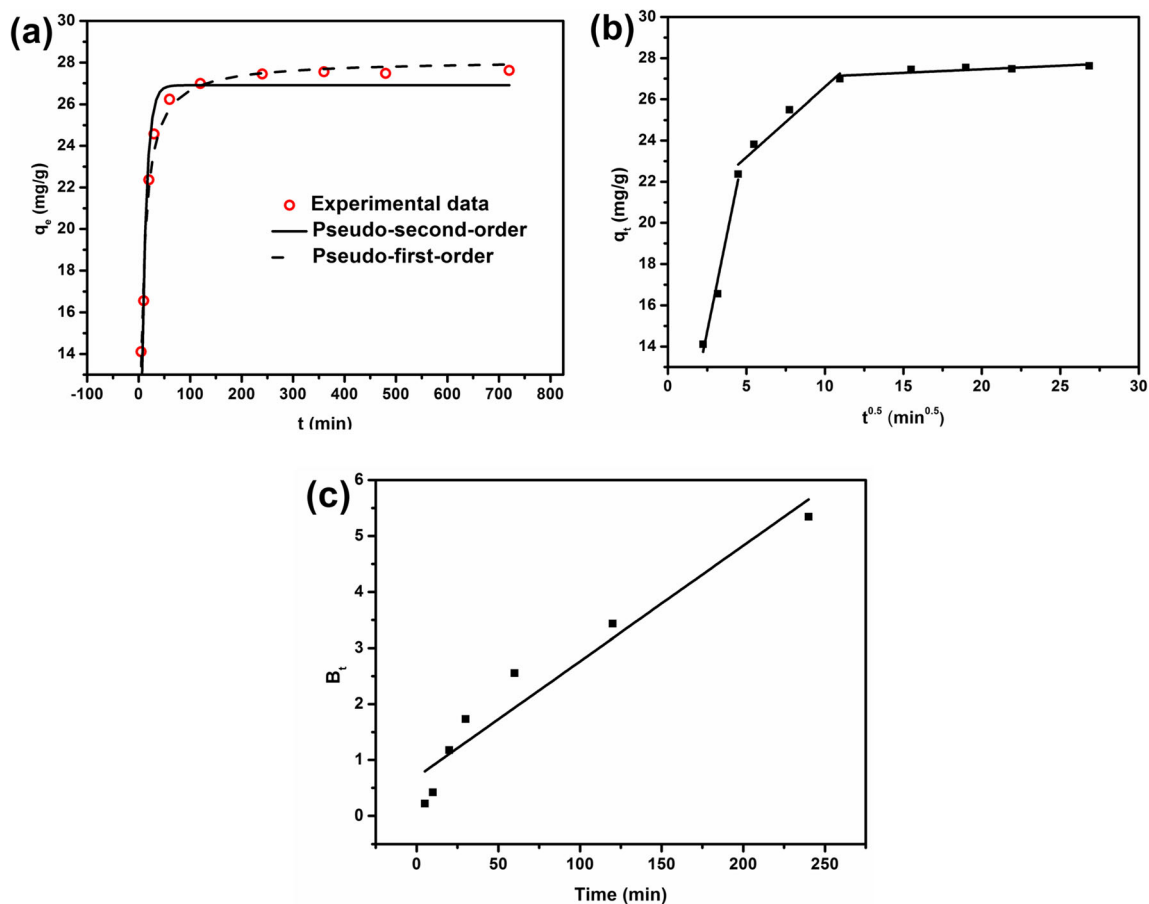


Fig. 4 Kinetic adsorption behavior of **a** pseudo-first-order model and pseudo-second-order model, **b** intra-particle diffusion model, and **c** Boyd model for adsorption phosphate onto MPVC-EDA-Ce

the plot of q_t versus $t^{0.5}$, indicating that the adsorption process of MPVC-EDA-Ce towards phosphate was multi-step (Lalley et al. 2016). Firstly, a fast adsorption process occurred due to the high concentration of phosphate and abundant binding sites, during which the adsorption of adsorbent towards phosphate was either through rapid migration to the external surface of the adsorbent or quick diffusion at the boundary (film diffusion). Then, the phosphate transferred into the adsorbent pores. Finally, the adsorption process reached an

equilibrium stage through the small pores' diffusion of the adsorbent and the chemical binding reaction of the adsorbate (Shokry and Hamad 2016).

The intra-particle diffusion model included film and pore diffusion, which was hard to identify the actual rate-limiting step of adsorption. Hence, as depicted in Fig. 4c, the Boyd model was used to interpret the kinetic data, indicating that the actual rate-controlling process was film diffusion because the straight line of B_t versus t did not cross the origin (Shokry and Hamad 2016).

Table 2 Kinetic parameters of phosphate adsorption onto prepared MPVC-EDA-Ce

q_e (mg/g)	Pseudo-first-order			Pseudo-second-order					
	k_1 (1/h)	q_e (mg/g)	R^2	k_2 (g/mg/h)	q_e (mg/g)	R^2			
27.530	0.107	26.906	0.921	0.00649	28.112	0.978			
Intra-particle diffusion model							Boyd		
K_{d1}	C_1	R_1^2	K_{d2}	C_2	R_2^2	K_{d3}	C_3	R_3^2	R^2
3.743	5.364	0.965	0.682	19.788	0.930	0.0347	26.765	0.623	0.922

Adsorption mechanism

The mechanism of phosphate adsorption onto the MPVC-EDA-Ce was analyzed by FT-IR, XPS, and zeta potential, respectively. The FT-IR spectra before and after phosphate adsorbed by MPVC-EDA-Ce are presented in Fig. 5. The strong broad band at around 3319 cm^{-1} was attributed to the stretching vibration of O-H and the band at 1624 cm^{-1} was attributed to the bending vibration of O-H, which could be overlapped by the characteristic peaks of N-H (Du et al. 2017). In addition, the peak at 3556 cm^{-1} was associated with the Ce-OH vibration on the surface of MPVC-EDA-Ce (Nodeh et al. 2017). The FT-IR spectrum of MPVC-EDA-Ce obviously changed after phosphate adsorption. The peaks of water molecules and hydroxyl groups became narrower as well as the peak of hydroxyl in $\text{Ce}(\text{OH})_3$ disappeared (Zhang et al. 2017). Additionally, there were new bands around 537 and 608 cm^{-1} (O-P-O bending vibration in PO_4^{3-} groups) and the band at 1048 cm^{-1} (P-O stretching vibration in PO_4^{3-} groups) after phosphate was adsorbed by MPVC-EDA-Ce (Zhang et al. 2016). These changes proved that PO_4^{3-} groups were adsorbed onto the adsorbent and suggested that the -OH groups on the surface of the adsorbent were substituted by the phosphate adsorbed by MPVC-EDA-Ce, further indicating the formation of inner-sphere surface complex between phosphate and the adsorbent (Zhang et al. 2017).

The XPS study was carried out to further reveal the possible mechanism of phosphate adsorption. The XPS spectra of MPVC-EDA-Ce before and after adsorbing phosphate are depicted in Fig. 6a, and found that there was a new peak of P 2p for MPVC-EDA-Ce adsorbing phosphate, which was consistent with the results of EDS and IR. As depicted in Fig. 6b, the Ce 3d spectrum of MPVC-EDA-Ce with or without phosphate adsorption exhibited two sets of bands located at $E_B[\text{Ce } 3d_{5/2}] = 882.1$ and 885.6 eV and $E_B[\text{Ce } 3d_{3/2}] = 900.4$ and $903.7.0\text{ eV}$. The binding energy of the Ce 3d spectrum after

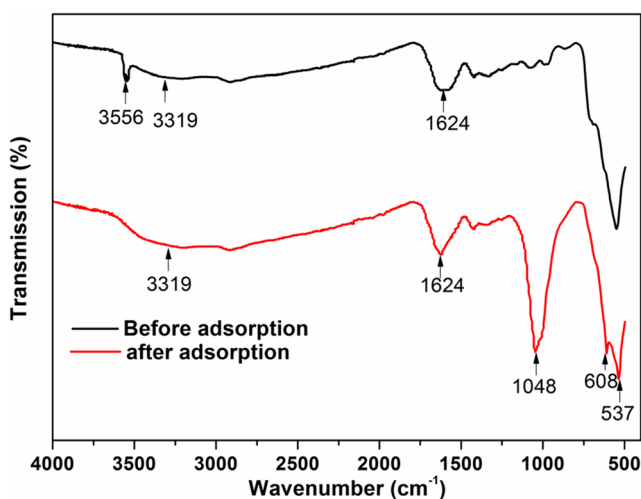


Fig. 5 FT-IR spectra of MPVC-EDA-Ce before and after adsorbing phosphate

phosphate adsorption moved towards higher energy to $E_B[\text{Ce } 3d_{5/2}] = 883.2$ and 886.7 eV and $E_B[\text{Ce } 3d_{3/2}] = 901.5$ and 904.8 eV (Koilaraj and Sasaki 2017), suggesting the strong affinity between phosphate and Ce(III) sites (Ge et al. 2016). Figure 6c shows that the binding energy of P 2p for PVC-EDA adsorbing phosphate was located at $\sim 134.6\text{ eV}$, but the peak of P 2p for NaH_2PO_4 was centered at $\sim 133.1\text{ eV}$. The slight shifts indicated that the adsorption between ammonium groups and phosphate was non-specific. Additionally, the higher binding energy (135.2 eV) of P 2p peak was observed in phosphate-loaded cerium (hydr)oxides, which suggested that there was the strong adsorption affinity for the formation of $\text{CePO}_4 \cdot x\text{H}_2\text{O}$. The XPS spectra for the phosphate adsorption onto MPVC-EDA-Ce with or without sulfate were also investigated in Fig. 6d and e. The broaden spectrum of P 2p peak for phosphate-loaded MPVC-EDA-Ce could be divided into two characteristic bands (phosphate-loaded quaternary ammonium group and $\text{CePO}_4 \cdot x\text{H}_2\text{O}$) considering the two functional adsorption sites (i.e., the quaternary ammonium group and cerium (hydr)oxides). The area fractions of phosphate-loaded quaternary ammonium group and $\text{CePO}_4 \cdot x\text{H}_2\text{O}$ were $\sim 43\%$ and $\sim 57\%$, respectively. However, the corresponding area fractions changed remarkably when the competing sulfate ion was added to the phosphate solution (sulfate/phosphate = 10). The area fractions corresponding to the amount of phosphate adsorbed onto the quaternary ammonium functional groups decreased from ~ 43 to $\sim 4.3\%$. And the area fractions corresponding to the amount of phosphate combined with the cerium site increased from ~ 57 to $\sim 95.7\%$, which further verified that there was a strong affinity between the cerium (hydr)oxides and phosphate (Qiu et al. 2017).

Additionally, the O 1s spectrum of MPVC-EDA-Ce before and after adsorbing phosphate is exhibited in Fig. 7a and b, respectively. The O 1s region could be divided into three bands located at 529.8 eV (oxygen bonded to metal), 531.2 eV (hydroxyl bonded to metal), and 532.8 eV (adsorbed water) according to the binding energies of different oxygen species. After adsorbing phosphate, the area ratio of oxygen bonded to metal increased from 53.2 to 83.1% , suggesting that the O-P bonds might be formed. However, the area ratio of hydroxyl bonded to metal decreased from 40.8 to 16.9% , indicating the -OH groups were substituted by phosphate adsorbed by MPVC-EDA-Ce (Ge et al. 2016). The results were in agreement with those of the FT-IR analysis.

The electrophoretic mobility measurement was also used to examine the phosphate adsorption mechanism. The point of zero charge (PZC) of PVC-EDA, MPVC-EDA, and MPVC-EDA-Ce was determined by their zeta potential in solutions with different pH values in Fig. S1. The zeta potentials of the adsorbents decreased with increasing pH values, and MPVC-EDA-Ce exhibited higher pH_{PZC} than that of MPVC-EDA and PVC-EDA. When $\text{pH} < \text{pH}_{\text{PZC}}$, the surface of adsorbents was positively charged, which facilitated the adsorption of negatively charged

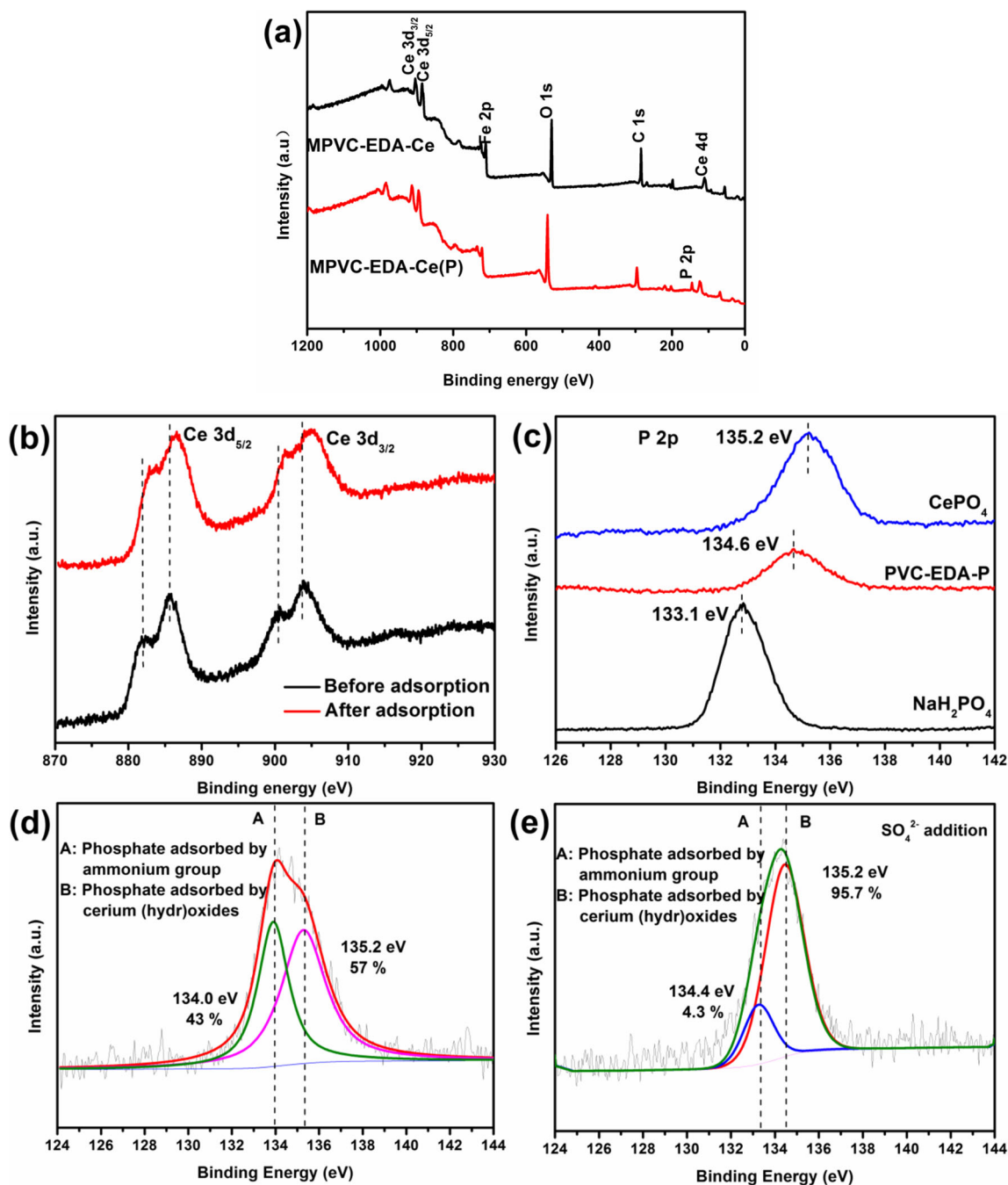


Fig. 6 **a** XPS survey scan of MPVC-EDA-Ce in the absence and presence of phosphate. **b** The $Ce\ 3d$ spectrum of MPVC-EDA-Ce in the absence and presence of phosphate. **c** The $P\ 2p$ spectral comparisons of

NaH_2PO_4 , phosphate-loaded PVC-EDA, and $CePO_4$ sample. **d**, **e** $P\ 2p$ spectra of the phosphate-loaded MPVC-EDA-Ce with or without sulfate additions

phosphate ions by electrostatic attraction. When $pH > pH_{pzc}$, the surface of adsorbents was negatively charged and it was unfavorable for phosphate adsorption via electrostatic attraction (Yang et al. 2018). Hence, MPVC-EDA-Ce with higher pH_{pzc} possessed good adsorption performance of phosphate over a wider pH range than MPVC-EDA and PVC-EDA. The zeta potentials of MPVC-EDA-Ce before and after adsorbing phosphate are shown in Fig. 8. The PZC of adsorbent decreased from

8.79 to 5.38 after adsorption phosphate. It was reported that PZC would not change if the outer-sphere complexes were formed since no specific reactions occurred between the adsorbent and phosphate. Correspondingly, the inner-sphere complexes might be formed for phosphate-loaded MPVC-EDA-Ce, because the PZC of MPVC-EDA-Ce shifted to a lower value after phosphate adsorption, indicating that the chemical reaction occurred between phosphate and the adsorbent (Zhang et al. 2010).

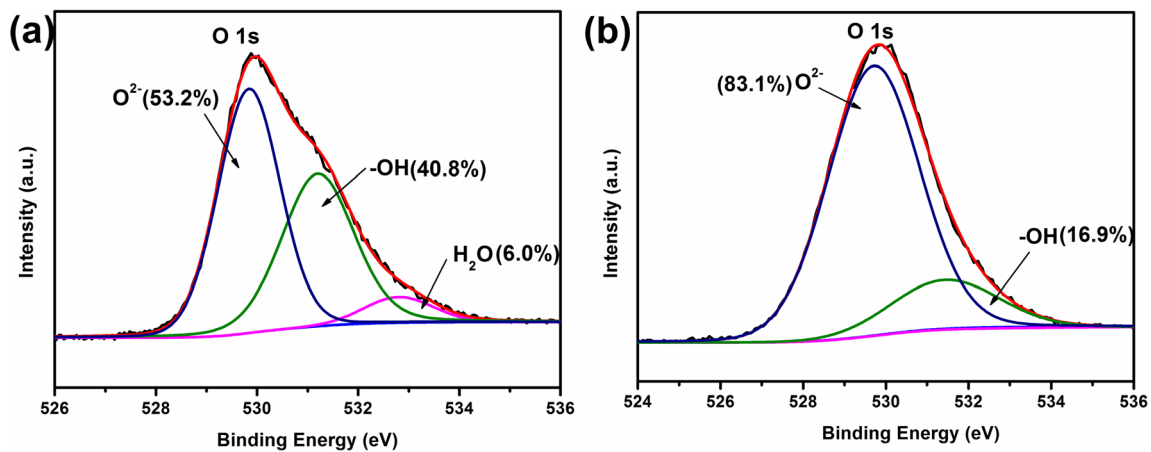


Fig. 7 a, b The O 1s spectrum of MPVC-EDA-Ce before and after adsorption

Effect of solution pH

The amount of phosphate adsorbed by MPVC-EDA-Ce as function of solution pH was discussed, because the solution pH could affect the adsorbent pH_{pzc} (the point of zero charge) and the species of phosphate. As shown in Fig. 9, the composite MPVC-EDA-Ce was highly pH-dependent. The amount of phosphate adsorbed by MPVC-EDA-Ce slightly increased as the solution pH increased and obtained the maximum amount of adsorption at pH 5.0 (28.35 mg/g). As the further increasing of pH, the amount of adsorption was significantly reduced and eventually reached 17.15 mg/g at pH 11. The results were related to the main existing form of phosphorus at different pH values and pH_{pzc} of adsorbent. $H_2PO_4^-$ was the dominant existing form of phosphorus in the pH range 3–7 (Jung et al. 2017), and HPO_4^{2-} was the dominant species within pH 8–12 (Ogata et al. 2016). Generally, it was easier for $H_2PO_4^-$ to be adsorbed on the surface of adsorbent than HPO_4^{2-} , because the former had the lower adsorption free energy as compared with the latter. At the solution $pH < pH_{pzc}$, the adsorbent surface was protonated with more positive-charged, which was favorable to adsorb the phosphate via

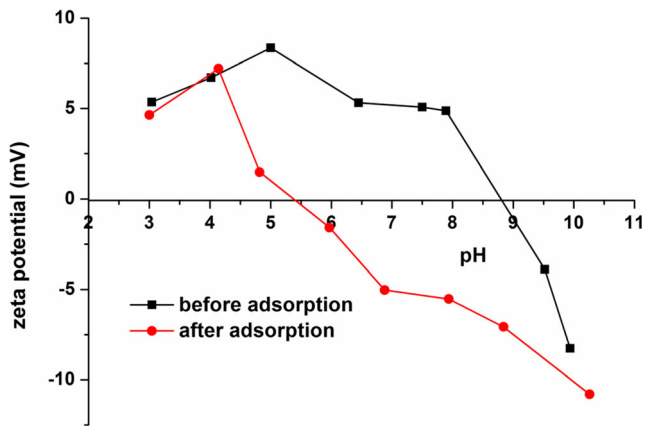


Fig. 8 Zeta potential curves of MPVC-EDA-Ce before and after adsorbing phosphate

electrostatic attraction (Unuabonah et al. 2017). However, at pH above pH_{pzc} , the adsorbent surface was deprotonated with more negatively charged as the solution pH increased, which makes the negatively charged phosphate ions difficult to adsorb owing to the repulsion reaction, and led to decrease of the adsorption capacity. Additionally, when the pH was greater than 9, the hydroxyl ions would occupy most of the active sites on the adsorbent surface, resulting in reducing the amount of phosphate adsorbed by the adsorbent.

Analyze the potential of real applications

Magnetic analysis

Magnetism played an important role in recovering materials from solution and the magnetic property of MPVC-EDA-Ce was tested. Magnetic hysteresis curve of MPVC-EDA-Ce is shown in Fig. S2. The adsorbent showed superparamagnetic since the magnetic hysteresis loops

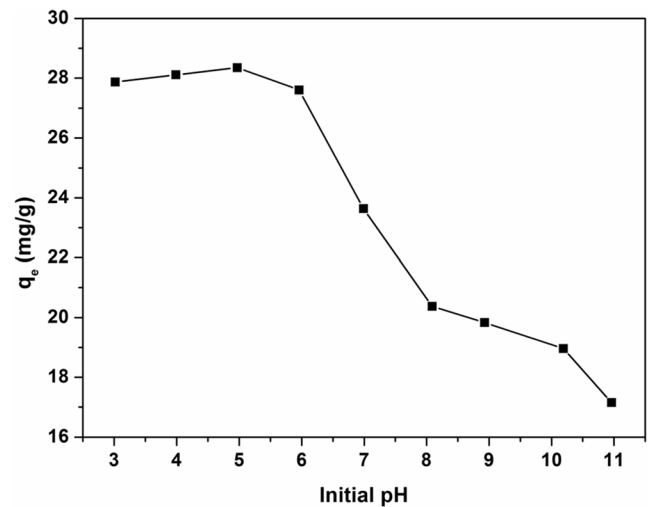


Fig. 9 Effect of pH on the amount of phosphate adsorbed by MPVC-EDA-Ce

were not observed (Zhang et al. 2017). The maximal saturation magnetization value of MPVC-EDA-Ce was 13.35 emug^{-1} , which facilitated the recovery of the adsorbent from the solution by the magnet (Fig. S3).

Ion leaching

The effect of pH on the stability of MPVC-EDA-Ce was also investigated. In Fig. S4, the concentration of the leached Fe and Ce was less than 0.05 mg/L within the tested pH range, indicating the good stability of MPVC-EDA-Ce as metal pollution would not be caused by the low metal leakage (Zhang et al. 2010).

Effect of competing anions

Adsorption selectivity was one of the important factors affecting phosphate adsorption. Some anions (i.e., sulfate, nitrate, and chloride) often coexisted in the wastewater with phosphate, which may occupy the active sites of the adsorbent surface. The effect of the competing anions on the amount of phosphate adsorbed by MPVC-EDA-Ce was further studied in Fig. 10a. The amount of phosphate adsorbed by MPVC-EDA-Ce significantly decreased when the molar ratio of the competing anion to phosphate increased, which may be due to

the fact that competitive anions occupied the functional adsorption site (quaternary ammonium groups and cerium (hydr)oxides) and caused a decrease in the amount of phosphate adsorption. Here, sulfate was chosen as a representative competing anion, because it showed a stronger competitive adsorption towards quaternary ammonium groups than others. And the contribution of each functional adsorption site (quaternary ammonium groups and cerium (hydr)oxides) to the phosphate adsorption could be quantified by comparison of adsorption capacities with and without sulfate. Figure 10 b showed the amount of phosphate adsorbed by the adsorbents in the presence of sulfate. When the molar ratio of sulfate to phosphate increased from 0 to 60, the adsorption capacity of MPVC-EDA-Ce towards phosphate declined from 27.28 to 18.41 mg/g , while that of MPVC-EDA and PVC-EDA declined from 8.29 to 1.24 mg/g and from 14.64 to 0.49 mg/g , respectively. The amount of the phosphate uptake onto cerium (hydr)oxides ($q_m(\text{Ce})$) was the difference between the adsorption amounts of MPVC-EDA-Ce and MPVC-EDA towards phosphate. And the amount of phosphate adsorbed by PVC-EDA represented the amount of phosphate uptake onto quaternary ammonium groups ($q_m(\text{N})$). Consequently, as shown in Fig. 10c, $q_m(\text{N})$ and $q_m(\text{Ce})$ occupied 43% and 57% of $q_m(\text{N} + \text{Ce})$ without any sulfate, respectively. However, $q_m(\text{N})$ and $q_m(\text{Ce})$ occupied around 4.2% and 95.8% of

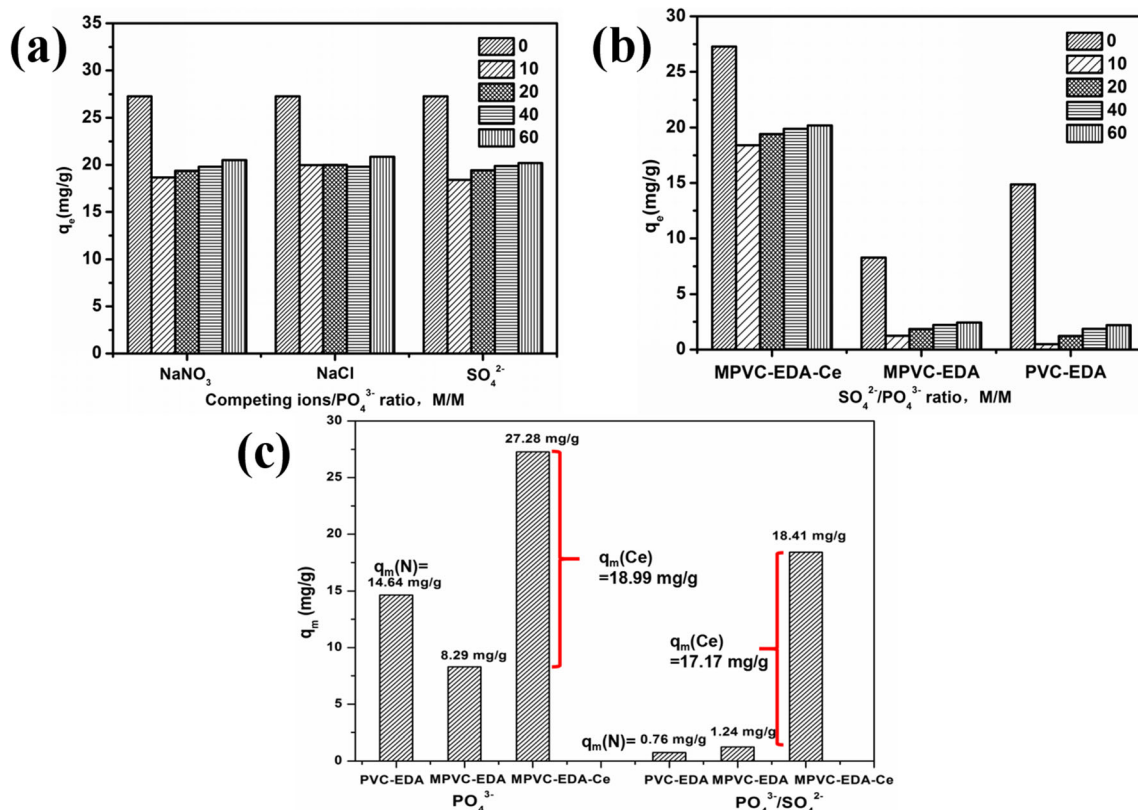


Fig. 10 a Effect of competing ions on the amount of phosphate adsorbed by MPVC-EDA-Ce. b Effect of sulfate on the amount of phosphate adsorbed by PVC-EDA, MPVC-EDA, and MPVC-EDA-Ce. c The

phosphate adsorption distributions of the PVC-EDA, MPVC-EDA, and MPVC-EDA-Ce with or without sulfate

$q_m(N + Ce)$ with excessive sulfate, respectively. The results were consistent with the XPS results for the phosphate adsorption onto MPVC-EDA-Ce in the presence or absence of sulfate (The phosphate uptake onto quaternary ammonium group and cerium sites declined from ~43 to ~4.3% and from ~57 to ~95.7% in the presence of sulfate, respectively). In addition, MPVC-EDA-Ce showed higher adsorption capacity towards phosphate than MPVC-EDA and PVC-EDA in a competitive background (Fig. 10b). The reason was that MPVC-EDA-Ce included two functional adsorption sites (the quaternary ammonium functional groups and cerium (hydr)oxides) for phosphate removal, while MPVC-EDA and PVC-EDA contained only quaternary ammonium functional groups as functional adsorption sites. The quaternary ammonium functional groups were positively charged and showed adsorption capacity towards negatively charged ions (e.g., phosphate and sulfate), which was a non-selective or non-specific adsorption process (Qiu et al. 2017). Therefore, for MPVC-EDA and PVC-EDA, the added competitive sulfate ions would occupy most adsorption sites of ammonium groups, which almost reduced the adsorption capacity of phosphate to zero. But there might be the formation of strong inner-sphere complexation between cerium (hydr)oxides and phosphate, which was a selective or specific adsorption process and could be explained by the principle of hard and soft acids and bases (the HSAB principle). Cerium (hydr)oxides were supposed to act as a soft Lewis acid and the phosphate acts as a soft Lewis base to represent electron pairs binding cerium atom, resulting in forming inner-sphere complexes. It was difficult for the coexisting anions to compete for active adsorption sites on encapsulated cerium (hydr)oxides (Qiu et al. 2015). Therefore, for MPVC-EDA-Ce, sulfate occupied only the adsorption sites of ammonium groups, while cerium (hydr)oxides exhibited preferable adsorption towards phosphate. Consequently, the adsorption capacity of MPVC-EDA-Ce towards phosphate was not reduced to zero with the addition of the competitive sulfate ions. The results indicated that the selectivity was provided by cerium (hydr)oxides rather than the quaternary ammonium groups.

Conclusion

In this study, MPVC-EDA-Ce with cerium (hydr)oxides and quaternary ammonium groups as two functional adsorption sites was prepared as a new phosphate adsorbent. The isotherm data followed Langmuir monolayer model and kinetics was simulated better by the pseudo-second-order model. The phosphate adsorption occurred rapidly and reached around 90% of the equilibrium adsorption amount within 30-min reaction time. The pH results suggested that the MPVC-EDA-Ce exhibited an excellent adsorption performance within a wide pH range with little cerium leaching, indicating its

potential for real use and environmental friendliness. Contributions of cerium (hydr)oxides and quaternary ammonium groups to the phosphate adsorption were quantified to be 43% and 57%, respectively. The adsorption of cerium (hydr)oxides towards phosphate was a selective or specific adsorption process, which was strong inner-sphere complexation, while positively charged quaternary ammonium groups-adsorbed phosphate was a non-selective or non-specific adsorption process, which was relatively weak electrostatic attraction. This work provided a new insight to design, construct, and evaluate novel phosphate adsorbents with two even more functional adsorption sites and study phosphate adsorption mechanism.

Funding information This work was supported by Guangdong Provincial Department of Science and Technology Application Research and Development Supporting Special Fund Project (2015B020235007) and the National Major Science and Technology Program for Water Pollution Control and Treatment (2013ZX07105-005).

Compliance with ethical standards

Conflict of interest The authors declare that they have no conflict of interest.

References

- Bui TH, Hong SP, Yoon J (2018) Development of nanoscale zirconium molybdate embedded anion exchange resin for selective removal of phosphate. *Water Res* 134:22–31
- Du X, Han Q, Li J, Li H (2017) The behavior of phosphate adsorption and its reactions on the surfaces of Fe–Mn oxide adsorbent. *J Taiwan Inst Chem Eng* 76:167–175
- Feng Y, Lu H, Liu Y, Xue L, Dionysiou DD, Yang L, Xing B (2017) Nano-cerium oxide functionalized biochar for phosphate retention: preparation, optimization and rice paddy application. *Chemosphere* 185:816–825
- Gan F, Zhou J, Wang H, Du C, Chen X (2009) Removal of phosphate from aqueous solution by thermally treated natural palygorskite. *Water Res* 43(11):2907–2915
- Ge X, Song X, Ma Y, Zhou H, Wang G, Zhang H, Zhang Y, Zhao H, Wong PK (2016) Fabrication of hierarchical iron-containing MnO₂ hollow microspheres assembled by thickness-tunable nanosheets for efficient phosphate removal. *J Mater Chem A* 4(38):14814–14826
- Goscianska J, Ptaszkowska-Koniarz M, Frankowski M, Franus M, Panek R, Franus W (2018) Removal of phosphate from water by lanthanum-modified zeolites obtained from fly ash. *J Colloid Interface Sci* 513:72–81
- Han C, Lalley J, Iyanna N, Nadagouda MN (2017) Removal of phosphate using calcium and magnesium-modified iron-based adsorbents. *Mater Chem Phys* 198:115–124
- Hong D, Yanling Z, Qianlin D, Junwen W, ZHANG K, Guangyue D, Xianmei X, Chuanmin D (2017) Efficient removal of phosphate from aqueous solution using novel magnetic nanocomposites with Fe₃O₄@ SiO₂ core and mesoporous CeO₂ shell. *J Rare Earths* 35(10):984–994
- Hu P, Liu Q, Wang J, Huang R (2017) Phosphate removal by Ce (III)-impregnated crosslinked chitosan complex from aqueous solutions. *Polym Eng Sci* 57(1):44–51

- Jung K-W, Jeong T-U, Choi J-W, Ahn K-H, Lee S-H (2017) Adsorption of phosphate from aqueous solution using electrochemically modified biochar calcium-alginate beads: batch and fixed-bed column performance. *Bioresour Technol* 244:23–32
- Jung K-W, Jeong T-U, Hwang M-J, Kim K, Ahn K-H (2015) Phosphate adsorption ability of biochar/mg–Al assembled nanocomposites prepared by aluminum-electrode based electro-assisted modification method with $MgCl_2$ as electrolyte. *Bioresour Technol* 198:603–610
- Koilraj P, Sasaki K (2017) Selective removal of phosphate using L-porous carbon composites from aqueous solutions: batch and column studies. *Chem Eng J* 317:1059–1068
- Lalley J, Han C, Li X, Dionysiou DD, Nadagouda MN (2016) Phosphate adsorption using modified iron oxide-based sorbents in lake water: kinetics, equilibrium, and column tests. *Chem Eng J* 284:1386–1396
- Long F, Gong JL, Zeng GM, Chen L, Wang XY, Deng JH et al (2011) Removal of phosphate from aqueous solution by magnetic Fe–Zr binary oxide. *Chem Eng J* 171(2):448–455
- Markeb AA, Ordosgoitia LA, Alonso A, Sánchez A, Font X (2016) Novel magnetic core–shell Ce–Ti@ Fe_3O_4 nanoparticles as an adsorbent for water contaminants removal. *RSC Adv* 6(62):56913–56917
- Nodeh HR, Sereshti H, Afsharian EZ, Nouri N (2017) Enhanced removal of phosphate and nitrate ions from aqueous media using nanosized lanthanum hydrous doped on magnetic graphene nanocomposite. *J Environ Manag* 197:265–274
- Ogata F, Imai D, Toda M, Otani M, Kawasaki N (2016) Properties of a novel adsorbent produced by calcination of nickel hydroxide and its capability for phosphate ion adsorption. *J Ind Eng Chem* 34:172–179
- Qiu G, Zhao Y, Wang H, Tan X, Chen F, Hu X (2019) Biochar synthesized via pyrolysis of *Broussonetia papyrifera* leaves: mechanisms and potential applications for phosphate removal. *Environ Sci Pollut Res*:1–11
- Qiu H, Liang C, Yu J, Zhang Q, Song M, Chen F (2017) Preferable phosphate sequestration by nano-La (III)(hydr) oxides modified wheat straw with excellent properties in regeneration. *Chem Eng J* 315:345–354
- Qiu H, Liang C, Zhang X, Chen M, Zhao Y, Tao T, Xu Z, Liu G (2015) Fabrication of a biomass-based hydrous zirconium oxide nanocomposite for preferable phosphate removal and recovery. *ACS Appl Mater Interfaces* 7(37):20835–20844
- Rathod M, Mody K, Basha S (2014) Efficient removal of phosphate from aqueous solutions by red seaweed, *Kappaphycus alvarezii*. *J Clean Prod* 84:484–493
- Robalds A, Dreijalte L, Bikovens O, Klavins M (2016) A novel peat-based biosorbent for the removal of phosphate from synthetic and real wastewater and possible utilization of spent sorbent in land application. *Desalin Water Treat* 57(28):13285–13294
- Samarasimhareddy M, Prabhu G, Vishwanatha TM, Sureshbabu VV (2013) PVC-supported palladium nanoparticles: an efficient catalyst for Suzuki cross-coupling reactions at room temperature. *Synth*. 45(09):1201–1206
- Sendrowski A, Boyer TH (2013) Phosphate removal from urine using hybrid anion exchange resin. *Desalination* 322:104–112
- Shen Z, Dong X, Shi J, Ma Y, Liu D, Fan J (2019) Simultaneous removal of nitrate/phosphate with bimetallic nanoparticles of Fe coupled with copper or nickel supported on chelating resin. *Environ Sci Pollut Res*:1–9
- Shokry H, Hamad H (2016) Effect of superparamagnetic nanoparticles on the physicochemical properties of nano hydroxyapatite for groundwater treatment: adsorption mechanism of Fe (II) and Mn (II). *RSC Adv* 6(85):82244–82259
- Su Y, Yang W, Sun W, Li Q, Shang JK (2015) Synthesis of mesoporous cerium–zirconium binary oxide nanoadsorbents by a solvothermal process and their effective adsorption of phosphate from water. *Chem Eng J* 268:270–279
- Tian S, Jiang P, Ning P, Su Y (2009) Enhanced adsorption removal of phosphate from water by mixed lanthanum/aluminum pillared montmorillonite. *Chem Eng J* 151(1–3):141–148
- Unuabonah EI, Agunbiade FO, Alfred MO, Adewumi TA, Okoli CP, Omorogie MO, Akanbi MO, Ofomaja AE, Taubert A (2017) Facile synthesis of new amino-functionalized agro-genic hybrid composite clay adsorbents for phosphate capture and recovery from water. *J Clean Prod* 164:652–663
- Xiong W, Tong J, Yang Z, Zeng G, Zhou Y, Wang D, Song P, Xu R, Zhang C, Cheng M (2017) Adsorption of phosphate from aqueous solution using iron-zirconium modified activated carbon nanofiber: performance and mechanism. *J Colloid Interface Sci* 493:17–23
- Yang Q, Wang X, Luo W, Sun J, Xu Q, Chen F, Zhao J, Wang S, Yao F, Wang D (2018) Effectiveness and mechanisms of phosphate adsorption on iron-modified biochars derived from waste activated sludge. *Bioresour Technol* 247:537–544
- Yoo H, Kwak S-Y (2011) TiO_2 -encapsulating PVC capable of catalytic self-suppression of dioxin emission in waste incineration as an eco-friendly alternative to conventional PVC. *Appl Catal, B* 104(1–2):193–200
- Yoon SY, Lee CG, Park JA, Kim JH, Kim SB, Lee SH, Choi JW (2014) Kinetic, equilibrium and thermodynamic studies for phosphate adsorption to magnetic iron oxide nanoparticles. *Chem Eng J* 236:341–347
- Zeng L, Li X, Liu J (2004) Adsorptive removal of phosphate from aqueous solutions using iron oxide tailings. *Water Res* 38(5):1318–1326
- Zhang C, Li Y, Wang F, Yu Z, Wei J, Yang Z, Ma C, Li Z, Xu Z, Zeng G (2017) Performance of magnetic zirconium-iron oxide nanoparticle in the removal of phosphate from aqueous solution. *Appl Surf Sci* 396:1783–1792
- Zhang S, Niu H, Cai Y, Zhao X, Shi Y (2010) Arsenite and arsenate adsorption on coprecipitated bimetal oxide magnetic nanomaterials: $MnFe_2O_4$ and $CoFe_2O_4$. *Chem Eng J* 158(3):599–607
- Zhang X, Wang W, Shi W, He J, Feng H, Xu Y, Cui F, Wang C (2016) Carbon nanofiber matrix with embedded $LaCO_3OH$ synchronously captures phosphate and organic carbon to starve bacteria. *J Mater Chem A* 4(33):12799–12806
- Zhou Y, Tang L, Yang G, Zeng G, Deng Y, Huang B, Cai Y, Tang J, Wang J, Wu Y (2016) Phosphorus-doped ordered mesoporous carbons embedded with Pd/Fe bimetal nanoparticles for the dechlorination of 2, 4-dichlorophenol. *Catal Sci Technol* 6(6):1930–1939

Publisher's note Springer Nature remains neutral with regard to jurisdictional claims in published maps and institutional affiliations.